NASA Conference Publication 2436

Advanced Earth-to-Orbit Propulsion Technology 1986

Volume I

Edited by
R. J. Richmond
George C. Marshall Space Flight Center
Huntsville, Alabama

S. T. Wu
The University of Alabama in Huntsville
Huntsville, Alabama

Proceedings of a conference held at
NASA George C. Marshall Space Flight Center
Huntsville, Alabama
May 13–15, 1986

National Aeronautics
and Space Administration

**Scientific and Technical
Information Branch**

1986

IMPELLER FLUID FORCES

C.E. Brennen, A.J. Acosta, T.K. Caughey
California Institute of Technology
Pasadena, California 91125

ABSTRACT

This paper addresses the issue of the steady and unsteady forces which may be imparted to a pump impeller by the through flow. The historical trend to increase the power density and speed of turbomachines has inevitably led to an increase in the number of fluid/structure interaction problems because the fluid forces scale like the square of the speed and thus become increasingly important relative to the structural strength. The present paper focuses on the radial forces acting on the impeller of a pump. Under the sponsorship of NASA, the authors have, over the past few years, conducted an extensive investigation of these forces and the associated hydrodynamically induced rotordynamic coefficients. A new facility, called the Rotor Force Test Facility was designed and constructed for the experimental component of this program. Measurements of the forces and rotordynamic coefficients have been made for a range of different impeller and volutes and include tests with the impeller of the high pressure oxygen turbopump (HPOTP) in the Space Shuttle Main Engine. Furthermore, tests have been conducted with different leakage flow geometries and, with different levels of pump cavitation. The paper will summarize these experimental measurements and the results of some theoretical analyses.

I. Introduction

The trend toward higher speed, higher power density liquid turbomachinery as exemplified by the SSME Turbopumps inevitably brings with it a greater sensitivity to operational problems in several fluid mechanical areas. Among these are the problems associated with cavitation, namely performance degradation, cavitation damage, noise and an array of additional potential instabilities. Furthermore the increased fluid stress loadings which increase like the square of the speed lead to an increase in the potential for fluid structure interaction problems. This paper addresses only one subset of the second class of problems namely those arising from the fluid-induced forces and the associated rotordynamic effects. We shall refer only briefly to the changes in these phenomena when the impeller cavitates.

The specific practical issues which this research addresses are as follows. First, large static radial forces can be caused by a lack of axisymmetry in the pump and its volute or casing. This can lead to excessive bearing loads and self-repositioning of the impeller within

the casing. Though there exist some previous data on these static forces and their dependence on flow rate and pump speed (Ref. 3,11,15), the data from the present program has identified the dependence on collector geometry (Ref. 6,7,8,14) and other factors such as the effect of cavitation (Ref. 13). Furthermore theoretical models have been developed (Ref. 1,2,21,22) which yield fairly accurate design-stage prediction of these forces.

The second practical problem arises because of the unsteady fluid forces which develop as a result of a whirl motion superimposed on the normal shaft rotation. The net result are fluid forces which can act on the impeller shaft to promote rotordynamic instability and thereby limit the safe operational speed of the pump (eg. Ref. 12). Similar fluid dynamical effects can arise in the turbomachinery seals (eg. Ref. 9) and new insights into this problem have resulted from the work of Professor Dara Childs. One of the characteristics of these fluid-induced rotordynamic problems is that they often lead to sub-synchronous whirl and hence the need to explore the full range of the ratio of whirl frequency to rotational frequency in the present experimental investigations. In both the high pressure hydrogen and oxygen pumps of the SSME these fluid-induced effects are important in determining the operational envelope. It should however be added that as a result of the SSME sponsored research it is now recognized that similar problems arise the context of other, less esoteric pumps (eg. boiler-feed pumps, Ref. 4).

Experimental measurement of the radial forces and rotordynamic coefficients forms the central core of the current research program. Even in the absence of cavitation the flows themselves are so complicated that they are beyond current computational or accurate analytical prediction; they involve unsteady turbulent flows in complex geometries. Approximate analytical models can be and have been developed (eg. Ref. 1,2) but these must be guided by the experimental observations. Thus we begin this review by a description of the facility constructed at Caltech and named the Rotor Force Test Facility.

However, a few notes on the notation are appropriate first. Instantaneous forces in the laboratory frame are decomposed into forces F_x, F_y in the x,y directions shown in figure 1. Like all other forces these are non-dimensionalized using $\rho\pi\omega^2 r_2^3 b_2$ where ρ is the fluid density, ω the rotational frequency (radian frequency) and r_2 and b_2 are the radius and width of the impeller discharge. Coordinates x,y are non-dimensionalized using the discharge radius, r_2. F_{ox}, F_{oy} are the time-averaged mean of F_x, F_y and therefore represent the steady component of the radial forces. In the experiments a circular whirl motion is superimposed on the impeller. This has a radius, ε, of 0.126 cm and radian frequency, Ω (figure 1). The instantaneous forces normal and tangential to the direction of whirl motion are denoted by F_T and F_N as shown. It follows that a positive F_T during forward whirl (positive Ω) implies a whirl-exciting hydrodynamic effect.

The non-dimensionalized instantaneous forces F_x and F_y are also decomposed into their steady and unsteady parts as follows:

$$\begin{matrix} F_x \\ F_y \end{matrix} = \begin{matrix} F_{ox} \\ F_{oy} \end{matrix} + \frac{1}{r_2}[A]\begin{matrix} x \\ y \end{matrix} = \begin{matrix} F_{ox} \\ F_{oy} \end{matrix} + \frac{\varepsilon}{r_2}[A(\Omega/\omega)]\begin{matrix} \cos \Omega t \\ \sin \Omega t \end{matrix} \qquad (1)$$

where the second form is specific to the circular whirl orbits used in the present experiments and [A] is the hydrodynamically-induced rotordynamic force matrix. Note that this must be a function of the frequency ratio, Ω/ω, as well as the mean operating condition of the pump given by the flow coefficient, ϕ = (Volume Flow Rate)/ $2\pi r_2^2 b_2 \omega$. The conventional approach of the rotordynamicist is to represent this dependence on Ω/ω by subdividing the matrix into components which depend on orbit position (x,y), on orbit velocity ($\dot{x}$, $\dot{y}$) and on orbit acceleration ($\ddot{x}$, $\ddot{y}$) where dots denote differentiation with respect to time. The common notation is

$$\begin{matrix} F_x \\ F_y \end{matrix} = \begin{matrix} F_{ox} \\ F_{oy} \end{matrix} - [M]\begin{matrix} \ddot{x} \\ \ddot{y} \end{matrix} - [C]\begin{matrix} \dot{x} \\ \dot{y} \end{matrix} - [K]\begin{matrix} x \\ y \end{matrix} \qquad (2)$$

where, here, the differentiation is with respect to dimensionless time, ωt. The matrices [M], [C] and [K] are then the hydrodynamically-induced mass, damping and stiffness matrices. It follows that

$$\begin{aligned} A_{xx} &= -K_{xx} - \frac{\Omega}{\omega} C_{xy} + \frac{\Omega^2}{\omega^2} M_{xx} \\ A_{xy} &= -K_{xy} + \frac{\Omega}{\omega} C_{xx} + \frac{\Omega^2}{\omega^2} M_{xy} \\ A_{yx} &= -K_{yx} - \frac{\Omega}{\omega} C_{yy} + \frac{\Omega^2}{\omega^2} M_{yx} \\ A_{yy} &= -K_{yy} + \frac{\Omega}{\omega} C_{yx} + \frac{\Omega^2}{\omega^2} M_{yy} \end{aligned} \qquad (3)$$

However it should be clearly understood that there is no reason to believe, a priori, that the hydrodynamic [A] matrix should have such a convenient quadratic dependence on Ω/ω. Indeed, some of the results clearly deviate from this in a way which suggests a substantial cubic term which, consistent with dynamic practice, we shall denote by a "jerk" matrix, [J].

Finally note that the above definitions imply

$$F_N = \tfrac{1}{2}(A_{xx} + A_{yy})$$
$$F_T = \tfrac{1}{2}(-A_{xy} + A_{yx}) \qquad (4)$$

and since virtually all the experimentally measured [A] matrices are skew-symmetric with $F_N = A_{xx} = A_{yy}$ and $F_T = -A_{xy} = A_{yx}$ discussion of the results can confined to the physically interpretable F_N and F_T.

2. Rotor Force Test Facility

The site of the facility is a pump test loop using water which contains systems for water quality control (temperature, air content), and for pressure and flow rate control and measurement as well as data acquisition systems. Since this facility has been described elsewhere (Ref. 6,16,5) we concentrate on the Rotor Force Test Facility (RFTF) installed within it and shown in figure 2. For a complete description of the RFTF the reader is referred to references 6,16,8,5. Briefly the RFTF consists of a housing (1) which can accommodate a range of different combinations of pump impellers (5) and collectors (volutes)(2). The flow to the inlet (3,4) is well-prepared, having a quite uniform velocity distribution and low turbulence without any swirl. The experimental objective was to impose well-controlled rotation and whirl motions on a very stiff impeller/shaft system and to directly measure the resulting fluid forces on the impeller. Thus we carry out a forced vibration experiment in order to study a specific aspect of a free vibration problem. The prescribed motions are produced as follows. The normal rotational motion is driven by a 20 HP DC motor through the main pump shaft (9). This rotates in a double bearing cartridge (7,8,11) in which the outer bearings are set eccentric to the the inner bearings. Hence rotation of the intermediate cartridge by means of a 2 HP DC "whirl" motor rotating the sprocket (9) through a chain drive produces the superimposed circular whirl motion. Flexibility in the main motor shaft permits this added motion. All of the experiments described herein use a whirl motion with a radius of 0.126 cm. The maximum speed of the main shaft is about 3600 rpm; that of the whirl motion is about 2500 rpm.

Both the main motor and the whirl motor are position and velocity controlled using optical encoders mounted to each shaft. This complex control system which is crucial to the success of the experiments operates as follows. A single, low frequency signal (frequency, ω/J where J is an integer) drives the entire system. Two frequency multipliers produce signals with frequencies ω and $I\omega/J$ where I is a second integer. The main motor is driven with position feedback control by the frequency, ω, which determines the pump speed. The whirl motor is similarly driven by the frequency, $\Omega = I\omega/J$, which becomes the whirl speed. Separate indices generated by the optical encoders ensure precise knowledge and control of the positions of the two motions the combination of which repeats at the basic frequency, ω/J. Both I and J are preset by thumb-wheel switches and therefore predetermine the important frequency ratio. This entire control system is also integrated into the data acquisition system which samples over at least one complete ω/J cycle.

Forces on the impellers have been measured in several ways. In the early experiments, only steady forces were measured by means of an "external balance" (Ref. 6,8) which required suspending the entire bearing cartridge on flexures. Forces were then measured in the non-rotating laboratory frame by strain-gauged elements. This straightforward procedure allowed the measurement (Ref. 6,8) of steady radial forces and hydrodynamic stiffness matrices, [K], and permitted educated design of the more complex "internal balance". Clearly the dynamic response of the external balance was severely limited because of the large suspended mass. Subsequently an "internal rotating balance" was fabricated; this is mounted on the main shaft immediately behind the impeller and directly measures the forces on the impeller ((6), figure 2). The four-post design of this internal balance involves 28 strain gauge bridges which measure all six force components. It has a flat frequency response up to about 150 Hz. The signals are lead through slip-rings to the data acquisition system. This internal balance permitted measurement of the complete rotordynamic matrix, [A], due to the impeller fluid forces. While the external balance could be calibrated using cables, pulleys and weights (Ref. 6) the internal balance required additional, more complex procedures in order to take into account dynamic calibration effects and tare forces (see Ref. 16,17). In summary each data point required four measurements at the same set of speeds namely (i) the forces when the impeller is running in water at the desired flow coefficient (ii) the forces when run in air (iii) the forces in water with the impeller removed and (iv) the forces in air with the impeller removed. The required hydrodynamic forces are then assessed from (i)-(ii)-(iii)+(iv) (see Ref. 16).

We should note that measurements have also been made of the circumferential pressure distributions in the flow leaving the impeller and in the leakage passage between the impeller shroud and the casing. Integration of these pressure distributions yielded radial forces acting on the impeller discharge and on the shroud. However, because of the very limited dynamic response of the manometers used for these pressure measurements, only steady radial forces and hydrodynamic stiffness matrices could be obtained by this means. The purpose of these pressure measurements was to try to locate the source of the hydrodynamic effects.

Finally it is important to comment on the impeller seal and the leakage flow. The discharge is partially sealed from the inlet by means of a face seal. During all measurements this seal is backed off to some desired clearance (usually 0.13 mm. but varied to determine its effect) to avoid interference with the force measurements. Thus, all tests involve a leakage flow back from the discharge to the inlet between the impeller shroud and the casing. The results will indicate that both this leakage flow and the main impeller through-flow contribute to the rotordynamic coefficients.

3. Impellers and Volutes

Many of the results presented here were obtained with a five bladed centrifugal pump impeller made and donated by Byron Jackson Pump Division, Borg Warner Industrial Products. This bronze impeller has a discharge diameter of 16.2 cm, a discharge blade angle of 23 deg. and a design specific speed of 0.57; it is designated Impeller X (see Ref. 1,2,6,8,16). A solid dummy impeller, Impeller S, having the same external profile as Impeller X as also tested. A second centrifugal impeller, Impeller Y had six blades and a discharge blade angle of 30 degrees. Tests were also performed with a purely radial centrifugal impeller whose front and back shrouds were flat disks; the purpose was to add to information on the effect of the fluid forces on the outside of the front shroud.

The high pressure liquid oxygen pump in the SSME has back-to-back impellers; Rocketdyne Division, Rockwell International and NASA provided us with one half of a prototype impeller (referred to as Impeller R). After necessary trimming to a discharge of 16.76 cm (from 17.4 cm) this impeller was also tested in the RFTF. It should be noted that this impeller incorporates an axial inducer which affects the results. Some tests have also been performed with a simple 9 degree helical inducer running alone.

In various combinations these impellers were tested with a spectrum of volutes and collectors as follows:

a. Volute A, a single exit, spiral volute with a base circle diameter of 18.3 cm, a spiral angle of 4 degree and designed to be well matched to Impeller X at a flow coefficient of 0.092. This combination of Impeller X and Volute A provides the central case with which other combinations are compared. (Ref. 6,8,1,2)

b. Volute B, an circular volute of uniform cross-sectional area. (Ref. 6,8)

c. Volute C, a spiral volute, smaller than Volute A with about one half of the cross-sectional area at the cutwater. (Ref. 1,2)

d. Volute E, made by Rocketdyne, a 17-vaned diffuser volute similar to that of the HPOTP. (Ref. 18)

e. Volutes D,F,G,H, a spiral volute capable of being fitted with various kinds of diffuser vanes. Volute D is the vaneless designation. (Ref. 16)

Not all of the possible combinations of impellers and volutes were tested. Neither will the present paper attempt to summarize all of the data obtained. Rather we present a cross-section of results designed to illustrate various phenomena.

4. Steady Radial Forces

Typical steady components of the radial forces for the Impeller X, Volute A combination as obtained using the external balance are shown in figure 3 (Ref. 8). These results are quite consistent with the previous measurements of Agostinelli, Nobles and Mockridge (Ref.3) and Iverson, Rolling and Carlson (Ref. 15). As anticipated in the non-dimensionalization, the forces do indeed scale with the square of the impeller speed. Furthermore the design objective that Volute A be "matched" to Impeller X is born out by the fact that the force approaches zero at the design flow coefficient of 0.092. Figure 4 illustrates the dependence on volute geometry by comparing the magnitude of the radial force for Volutes A and B. Hypothetically the circular Volute B would only be well matched at zero flow; note that the results do exhibit the minimum radial force at shut off. Theoretical results due to Domm and Hergt (Ref. 11) and Colding-Jorgensen (Ref. 10) are also shown in figure 2 and yield fair estimates of the forces. However these theories, being based on the modelling of an impeller by a source-vortex and using potential flow, are of limited applicability.

Typical pressure distributions for the Impeller X discharge flow into Volute A are shown in figure 5; for more detail on the variation of the pressure distribution with flow rate and volute shape the reader is referred to Ref. 1,6. Also shown in this graph are theoretical predictions based on guided flow through the impeller and a one-dimensional treatment of the volute (Ref. 1,2). This same theory was extended to calculations of the rotordynamic coefficients (see below). Integration of the experimental pressure distributions yielded radial forces in good agreement with the internal balance measurement as shown in figure 6 (Ref. 1,2). Hence the conclusion that it is primarily the non-uniformity in the pressure and not the non-uniformity in the momentum flux which gives rise to the radial force. This was confirmed by the theoretical results whose agreement with the experiments is demonstrated in figure 6.

With respect to the leakage flow outside the front shroud it should be noted that two separate sets of experiments were conducted (Ref. 1,2). A set of additional rings were installed as protrusions from the volute in order to effect greater isolation of the impeller discharge from the fluid filled "cavity" between the front shroud and the casing; the axial clearance between the rings and the impeller was 0.12 mm (Ref. 1,2). In the absence of these rings measurements in the cavity indicated that the pressure distributions on the outside of the front shroud were significantly effected by the asymmetry in the impeller discharge pressures. And thus the fluid in this region contributed significantly to the radial force. The data of figures 3 and 4 were obtained without the rings. On the other hand installation of the rings increase the isolation of the cavity from the discharge pressure asymmetries and then the contribution of the "cavity" pressure to the radial force is small. However this does not decrease the radial force because the leakage flow tends to smooth out asymmetries in the discharge pressure. Hence restriction of the leakage also

amplifies the radial force on the impeller discharge. The data of figures 5 and 6 was obtained with the rings installed. In summary, the primary contribution to the radial force is the asymmetry in the impeller discharge pressure distribution. However the pressure on the outside of the front shroud may also contribute if there is no restriction at the discharge end of this flow path. Counteracting this effect is the fact that increased leakage flow tends to smooth out the discharge pressure asymmetry.

Diffuser vanes of the typical low solidity appear to have relatively little qualitative effect on the radial force which is primarily due to the volute asymmetry. For example the radial force due to Impeller X in Volute E were similar to those in Volute A (Ref. 18).

On the other hand cavitation can cause major changes in the radial force magnitude and direction (Ref. 13). The cavitation performance of the Impeller X/Volute A combination is shown in the upper part of figure 7 for three different flow coefficients; note the head breakdown for cavitation numbers, σ, in the range 0.2 to 0.3. The corresponding changes in the magnitude and direction of the radial force are shown in the lower part of figure 7. Note that these changes only occur at cavitation numbers for which there is a significant change in pump head. Since pumps operating near breakdown often exhibit substantial head fluctuations it follows that the radial forces under these circumstance may also fluctuate, resulting in substantial fluctuations in the bearing loads.

5. Hydrodynamically-Induced Rotordynamic Motion

Figure 8 presents typical values of the four [A] matrix elements as functions of the frequency ratio, Ω/ω; this for Impeller X/Volute A at 1000 rpm and the design flow coefficient of 0.092. This demonstrates the ubiquitous skew-symmetric characteristic of the results in which $A_{xx} = A_{yy} = F_N$, $A_{yx} = -A_{xy} = F_T$. This skew-symmetry indicates that the hydrodynamic effects which give rise to these forces are essentially rotationally symmetric. Since this was true of all the results presented we may confine our presentation to F_N and F_T which are more readily visualized. Figure 9 presents data for F_N and F_T at different shaft speeds and confirms the scaling of the forces with speed implicit in the non-dimensionalization.

The most significant feature of these results is the existence of an interval of frequency ratio in which F_T is in the same direction as the whirl motion and the fluid force promotes whirl. In figure 9 this interval is $0 < \Omega/\omega < 0.4$. As the flow coefficient is decreased below the design value, F_N and F_T change but only by modest amounts (Ref. 16,17). Nevertheless the upper limit of this interval increases with decreasing Φ, becoming about 0.6 at $\Phi = 0.06$ (Ref. 17). With Impeller A, the F_N, F_T characteristics were similar with all the volutes tested including those with diffuser vanes. Table I presents a summary of the hydrodynamic stiffness, damping and mass matrices obtained by fitting quadratics to the functions $A(\Omega/\omega)$. Only when the volute was

removed (Volute N) or when the dummy Impeller S was used were there substantial qualitative changes in [K], [C] and [M].

In addition to the direct force measurements, stiffness matrices, [K], could be obtained from discharge pressure distributions measured with the impeller placed at four different locations around the whirl orbit. Figure 10 presents typically differences in these pressure distributions for two such impeller locations (Ref. 1,2). Also shown are the theoretical distributions. Despite the differences between the experimental and theoretical data the shift in the distributions due to the change in impeller location are similar. Distributions like these lead to the typical stiffness matrices shown in figure 11 where direct measurements, integrated pressure data and theory are compared. Note that the direct measurements are substantially larger in magnitude than either the integrated discharge pressure or the theoretical results for the flow through the impeller. The same is true of the results in figure 11. We tentatively conclude that the leakage flow effects on the impeller shroud contribute significantly to the rotordynamic coefficients. Returning to figure 10 we note that the Adkins and Brennen theory agrees fairly well with the experimental integrated pressure results. Colding-Jorgensen's theory predicts diagonal terms of the right order but produces cross-coupling terms which are too small. Adkins and Brennen theoretical values for the complete [A] matrix are compared in figure 12 (for $\Phi = 0.092$) with direct measurements. Note that the form of the variation with frequency ratio is in agreement with the experiments and it is quite possible that the discrepancy can be attributed to leakage flow effects.

As with the steady radial forces, cavitation sufficient to cause head degradation also causes substantial changes in the rotordynamic coefficients. Ref. 13 presents this result for the stiffness, [K], as a function of cavitation number. The diagonal terms decrease by as much as a factor of two when breakdown occurs; on the other hand the off-diagonal terms increase by a smaller factor.

The SSME HPOTP Impeller R has yielded preliminary rotordynamic coefficients whose form is illustrated by figure 13 (Ref. 14). Most significant is the additional peak in F_T at frequency ratios of the order of $0.3 \rightarrow 0.4$. This feature, which enlarges the frequency ratio interval in which the hydrodynamic forces are destabilizing, is believed to be caused by forces on the unshrouded inducer. Preliminary measurements on induces tested without an impeller has indicated similar peaks in F_T.

6. Concluding Remarks

The research described in this paper has investigated two important consequences of the radial forces exerted on a pump by the fluid. Steady radial forces which can cause large bearing loads result from rotational asymmetry in the flow due to asymmetry in the volute (or inlet flow through this aspect has not been investigated). These forces are shown to be the result of non-uniformity in the

impeller discharge pressure distribution. A theoretical model has been developed which yields good agreement with the experimental measurements. Further experiments to investigate the effects of cavitation, show that degradation in pump head leads to corresponding changes in the magnitude and direction of the steady radial forces.

The second phenomena examined are the hydrodynamic contributions to the rotordynamic coefficients for the impeller. It is shown that there exists a range of subsynchrous whirl frequencies for which the hydordynamic forces promote whirl. This range increases as the flow rate is reduced below the design value. Data for the hydrodynamic stiffness, damping and mass matrices are presented for various impeller/volute combinations. The evidence suggests that both the main flow through the impeller and the leakage flow back from discharge to inlet outside of the front shroud contribute to these hydrodynamic coefficients. The theoretical model for the main impeller flow yields values which are smaller than the experimental data; further theoretical and experimental work on the leakage flow may elucidate the situation. Finally it is observed that either the addition of an inducer or the presence of cavitation can substantially effect these hydrodynamically-induced rotordynamic coefficients.

7. Acknowledgement

The authors are indebted to the NASA George Marshall Space Flight Center, Huntsville, Alabama for continued sponsorship of this research under contract NAS8-33108. Several former graduate students at Caltech including D.S. Chamieh, B. Jery and D.R. Adkins made major contributions to this work; we are grateful to them as we are to current graduate students R. Franz and N. Arndt. We also acknowledge the help given by undergraduates, W. Goda of Caltech and D. Brennen of UCSD.

REFERENCES

[1] Adkins, D.R., "Analyses of Hydrodynamic Forces on Centrifugal Pump Impellers". Ph.D. Thesis, California Institute of Technology, 1986.

[2] Adkins, D.R. and Brennen, C.E., "Analyses of Hydrodynamic Radial Forces on Centrifugal Pump Impellers". Submitted to ASME J. Fluids Engineering.

[3] Agostinelli, A., Nobles, D., and Mockridge, C.R., "An Experimental Investigation of Radial Thrust in Centrifugal Pumps", Trans. ASME, J. of Engr. for Power, Vol. 82, pp. 120-126, April 1960.

[4] Bolleter, U., and Wyss, A., "Measurement of Hydrodynamic Interaction Matrices of Boiler Feed Pump Impellers", Presented at ASME Design Engineering Divsion Conference and Exhibit on Mechanical Vibration and Noise, Cincinnati OH, Sept. 10-13, 1985.

[5] Brennen, C.E., Acosta, A.J., and Caughey, T.K., "A Test Program to Measure Fluid Mechanical Whirl-Excitation Forces in Centrifugal Pumps", First Workshop on Rotordynamic Instability Problems in High Performance Turbomachinery, Texas A&M University, NASA Conf. Pub. 2133, pp. 229-235, 1980.

[6] Chamieh, D.S., "Forces On A Whirling Centrifugal Pump-Impeller", Ph.D. Thesis, Division of Engineering and Applied Sciences, California Institute of Technology, 1983.

[7] Chamieh, D.S., Acosta, A.J., Brennen, C.E., Caughey, T.K., and Franz, R., "Experimental Measurements of Hydrodynamic Stiffness Matrices for a Centrifugal Pump Impeller", 2nd Workshop on Rotor- dynamic Instability Problems in High Performance Turbomachinery, Texas A&M University, NASA Conf. Pub. 2250, pp. 382-398, May 10-12, 1982.

[8] Chamieh, D.S., Acosta, A.J., Brennen, C.E. and Caughey, T.K., "Experimental Measurements of Hydrodynamic Radial Forces and Stiffness Matrices for a Centrifugal Pump Impeller", J. Fluids Engineering, 1985, Vol. 107, pp. 307-315.

[9] Childs, D.W., "Finite Length Solutions for Rotordynamic Coefficients of Turbulent Annular Seals", ASME J. of Lubrication Technology, Vol. 105, pp. 437-444, July 1983.

[10] Colding-Jorgensen, J., "The Effect of Fluid Forces on Rotor Stability of Centrifugal Compressors and Pumps", First Workshop on Rotordynamic Instability Problems in High Performance Turbomachinery, Texas A&M University, NASA Conf. Pub. 2133, pp. 249-266, May 12-14, 1980.

[11] Domm, H. and Hergt, P., "Radial Forces on Impeller of Volute Casing Pumps", in "Flow Research on Blading", Dzung, L.S., ed., Elsevier Publ. Co., 1970, pp. 305-321.

[12] Ehrich, F., and Childs, D., "Self-Excited Vibration in High Performance Turbomachinery", Mech. Engr., Vol. 106, No. 5, pp. 66-79, May 1984.

[13] Franz, R., Brennen, C.E., Acosta, A.J., and Caughey, T.K., "On the Effect of Cavitation on the Radial Forces and Hydrodynamic Stiffness of a Centrifugal Pump", Rotordynamic Instability Problems in High Performance Turbomachinery", Texas A&M University, NASA Conf. Publ., June 1986 (to be presented)

[14] Franz, R. and Arndt, N., "Measurements of Hydrodynamic Forces on the Impeller of the HPOTP of the SSME", California Institute of Technology, Div. of Eng. & Appl. Sci., Report No. E249.2

[15] Iversen, H.W., Rolling, R.E., and Carlson, J.J., "Volute Pressure Distribution, Radial Force on the Impeller and Volute Mixing Losses of a Radial Flow Centrifugal Pump", Trans. ASME, J. of Engr. for Power, Vol. 82, pp. 136-144, April 1960.

[16] Jery, B. "Experimental Study of Unsteady Hydrodynamic Force Matrices on Whirling Centrifugal Pump-Impellers", Ph.D. Thesis, Division of Engineering and Applied Sciences, California Institute of Technology, 1986.

[17] Jery, B., Acosta, A.J., Brennen, C.E., and Caughey, T.K., "Hydro- dynamic Impeller Stiffness, Damping and Inertia in the Rotordynamics of Centrifugal Flow Pumps", Rotordynamic Instability Problems in High Performance Turbomachinery, Texas A&M University, NASA Conf. Pub. 2338, pp. 137-160, May 28-30, 1984.

[18] Jery, B. and Franz, R., "Stiffness Matrices for the Rocketdyne Diffuser Volute". Division of Eng. & Appl. Science, California Institute of Technology, Report No. E249.1, 1982.

[19] Ohashi, H., and Shoji, H., "Lateral Fluid Forces Acting on a Whirling Centrifugal Impeller in Vaneless and Vaned Diffuser", Rotordynamic Instability Problems in High Performance Turbomachinery, Texas A&M University, NASA Conf. Pub. 2338, pp. 109-122, May 28-30, 1984.

[20] Shoji, H., and Ohashi, H., "Fluid Forces on Rotating Centrifugal Impeller with Whirling Motion", First Workshop on Rotordynamic Instability Problems in High Performance Turbomachinery, Texas A&M University, NASA Conf. Pub. 2133, pp. 317-328, 1980.

[21] Tsujimoto, Y., Acosta, A.J., and Brennen, C.E., "Two-Dimensional Unsteady Analysis of Fluid Forces on a Whirling Centrifugal Impeller in a Volute", Rotordynamic Instability Problems in High Performance Turbomachinery, Texas A&M University, NASA Conf. Pub. 2338, pp. 161-171, May 28-30, 1984.

[22] Tsujimoto, Y., Acosta, A.J. and Brennen, C.E., "Theoretical Study of the Fluid Forces on a Centrifugal Pump Impeller Rotating and Whirling in a Volute". Submitted to ASME J. Fluids Engineering.

VOLTE SPEED	IMPEL. PHI	Kxx Kyx	Kxy Kyy	Cxx Cyx	Cxy Cyy	Mxx Myx	Mxy Myy
A 500	X 0.092	-2.375 -1.094	1.100 -2.640	2.934 -8.141	7.685 3.341	6.906 0.358	-0.697 6.137
A 1000	X 0.092	-2.681 -1.220	1.011 -2.532	2.894 -8.477	8.568 3.668	6.166 0.294	-0.774 6.382
A 1500	X 0.092	-2.541 -1.078	0.901 -2.398	2.877 -8.764	8.709 3.116	6.979 0.628	-1.114 6.761
A 2000	X 0.092	-2.687 -1.239	1.062 -2.596	2.807 -9.066	9.108 3.009	6.928 0.648	-0.693 7.110
E 1000	X 0.000	-1.893 -0.138	0.145 -1.387	3.449 -7.379	7.835 3.350	6.183 -0.923	0.433 7.483
E 1000	X 0.060	-2.805 -0.992	1.643 -2.710	3.662 -9.421	9.647 3.811	6.581 1.021	-0.998 7.259
E 1000	X 0.092	-2.699 -0.967	1.104 -2.592	3.728 -8.846	9.071 3.871	6.222 0.926	-0.886 6.978
E 1000	X 0.145	-2.546 -1.157	1.169 -2.343	4.181 -7.770	8.898 4.127	5.624 0.437	-0.661 6.774
N 1000	X 0.060	-0.646 -0.739	0.611 -0.462	1.125 -3.575	3.627 1.337	4.249 -2.090	1.265 4.567
D 1000	X 0.060	-2.996 -1.165	1.669 -2.725	2.626 -9.193	9.298 3.992	6.254 -0.102	-0.401 6.683
F 1000	X 0.060	-3.454 -1.325	1.386 -3.337	3.490 -9.538	9.484 3.781	6.138 0.541	-0.904 6.357
G 1000	X 0.060	-3.469 -1.239	1.357 -3.228	3.314 -9.229	8.991 3.532	5.388 0.195	-0.589 6.122
H 1000	X 0.060	-3.523 -1.317	1.349 -3.333	3.568 -10.351	10.329 3.932	6.991 0.485	-0.819 7.482
E 1000	Y 0.092	-2.900 -0.776	0.922 -2.714	3.269 -8.331	8.724 3.483	5.250 0.724	-0.763 5.745
A 1000	S 0.000	-0.628 -0.516	0.302 -0.213	1.685 -3.874	3.795 2.857	6.282 -0.161	-0.337 6.882

TABLE I.

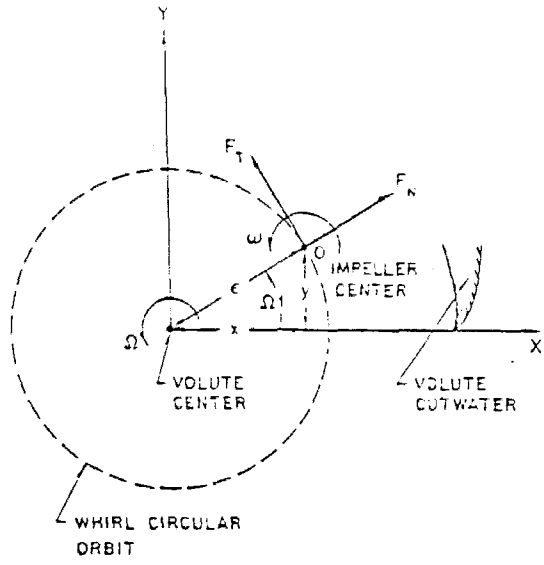

Figure 1 Coordinate systems and notation in plane perpendicular to the axis of rotation of the impeller.

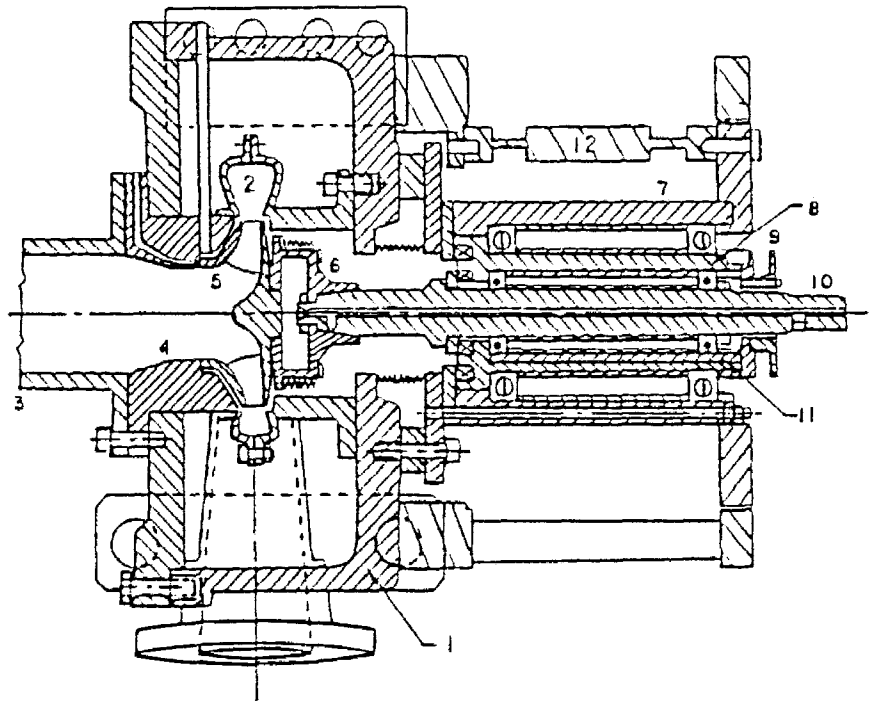

Figure 2 Rotor Force Test Facility: (1) pump housing, (2) volute, (3) inlet duct, (4) inlet bell, (5) impeller, (6) internal balance (7,8,11) double bearing system (9) whirl motion sprocket (12) external balance flexure (pinned when using internal balance).

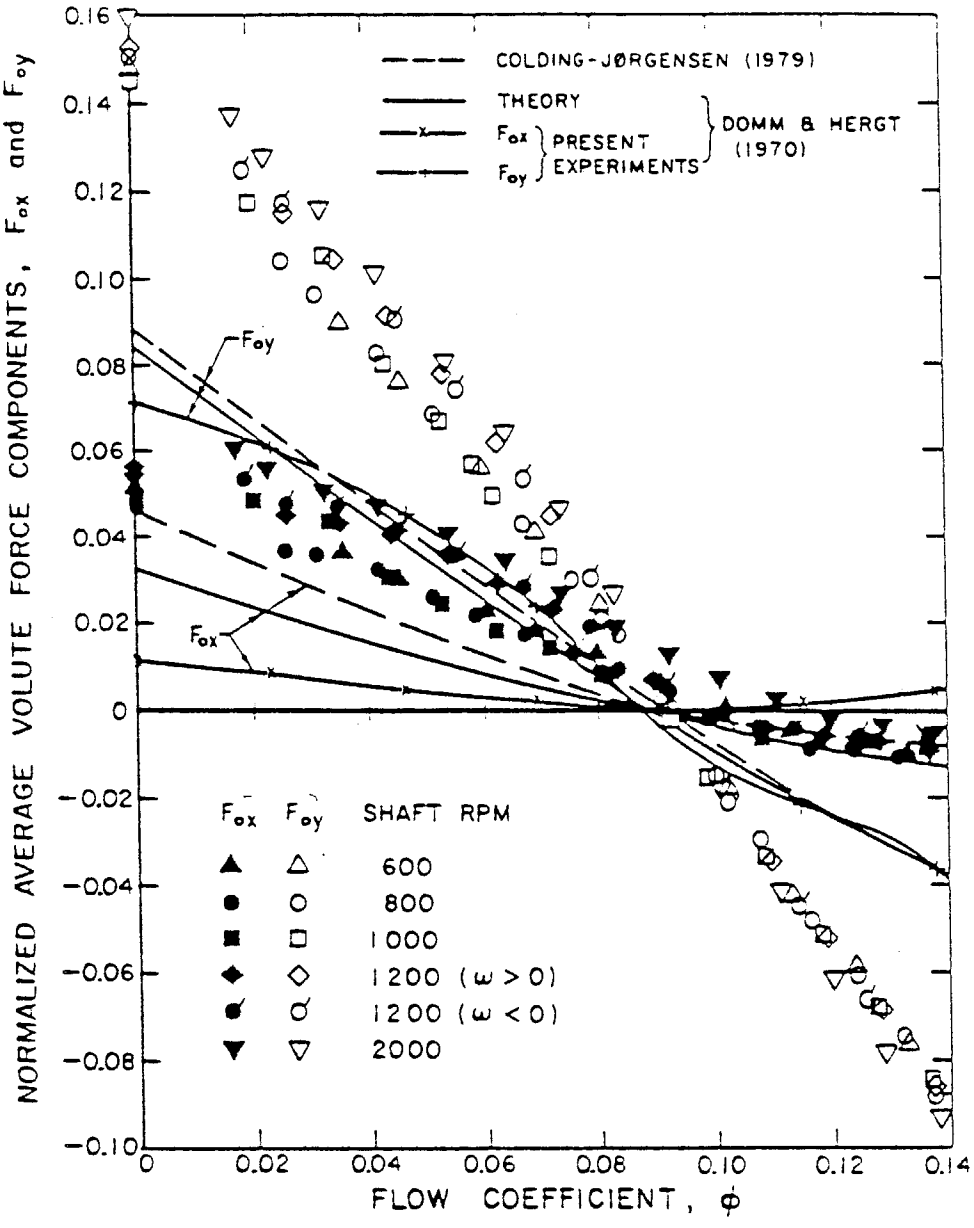

Figure 3 Normalized average radial force components, F_{ox} and F_{oy} for Impeller X/Volute A as a function of flow coefficient, Φ, at various shaft speeds and a face seal clearance of 0.14 mm. Also shown are some results by Domm and Hergt (Ref. 11) and Colding-Jorgensen (Ref. 10) for a similar impeller/volute combination.

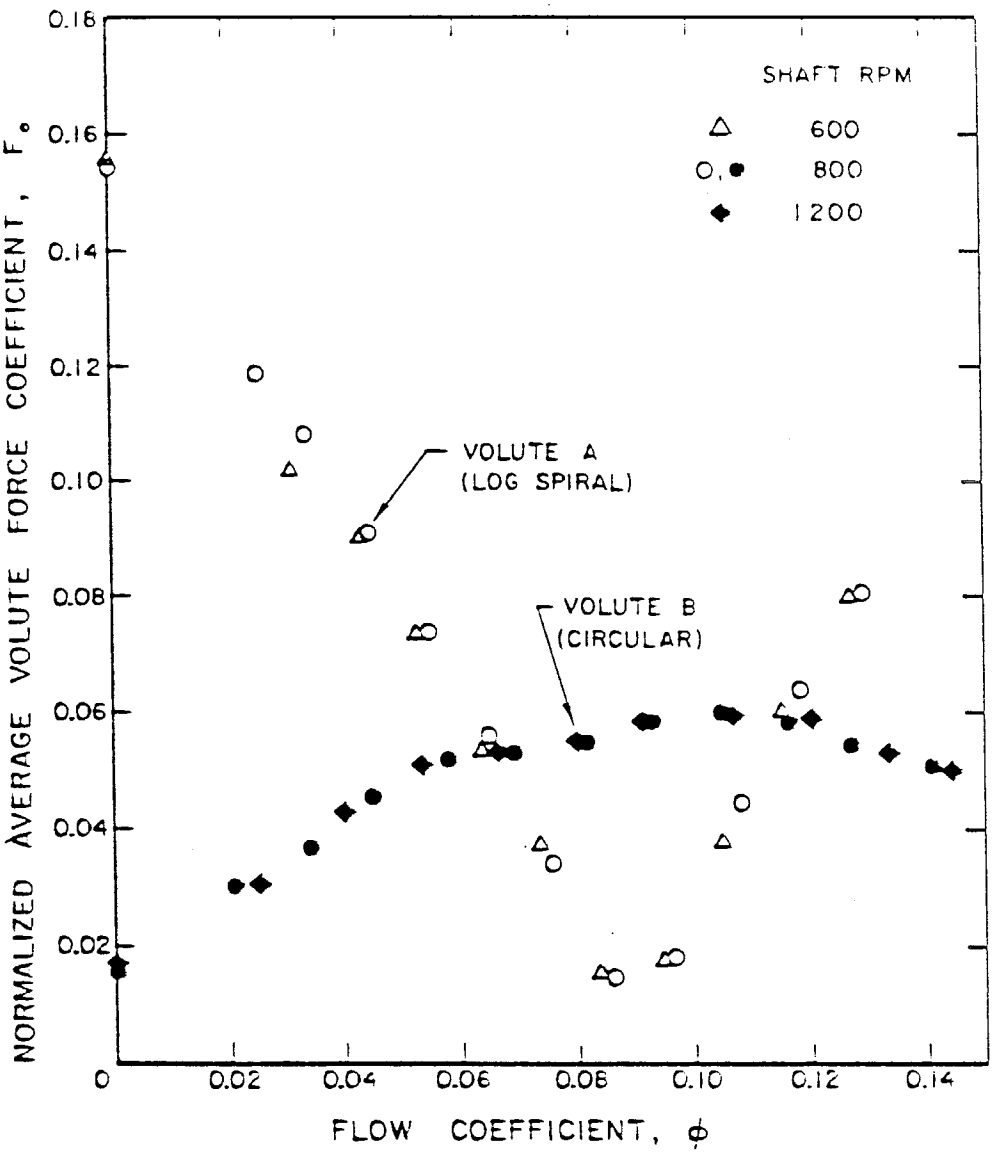

Figure 4 Comparison of the radial forces (plotted as in figure 3) for Impeller X with Volutes A and B.

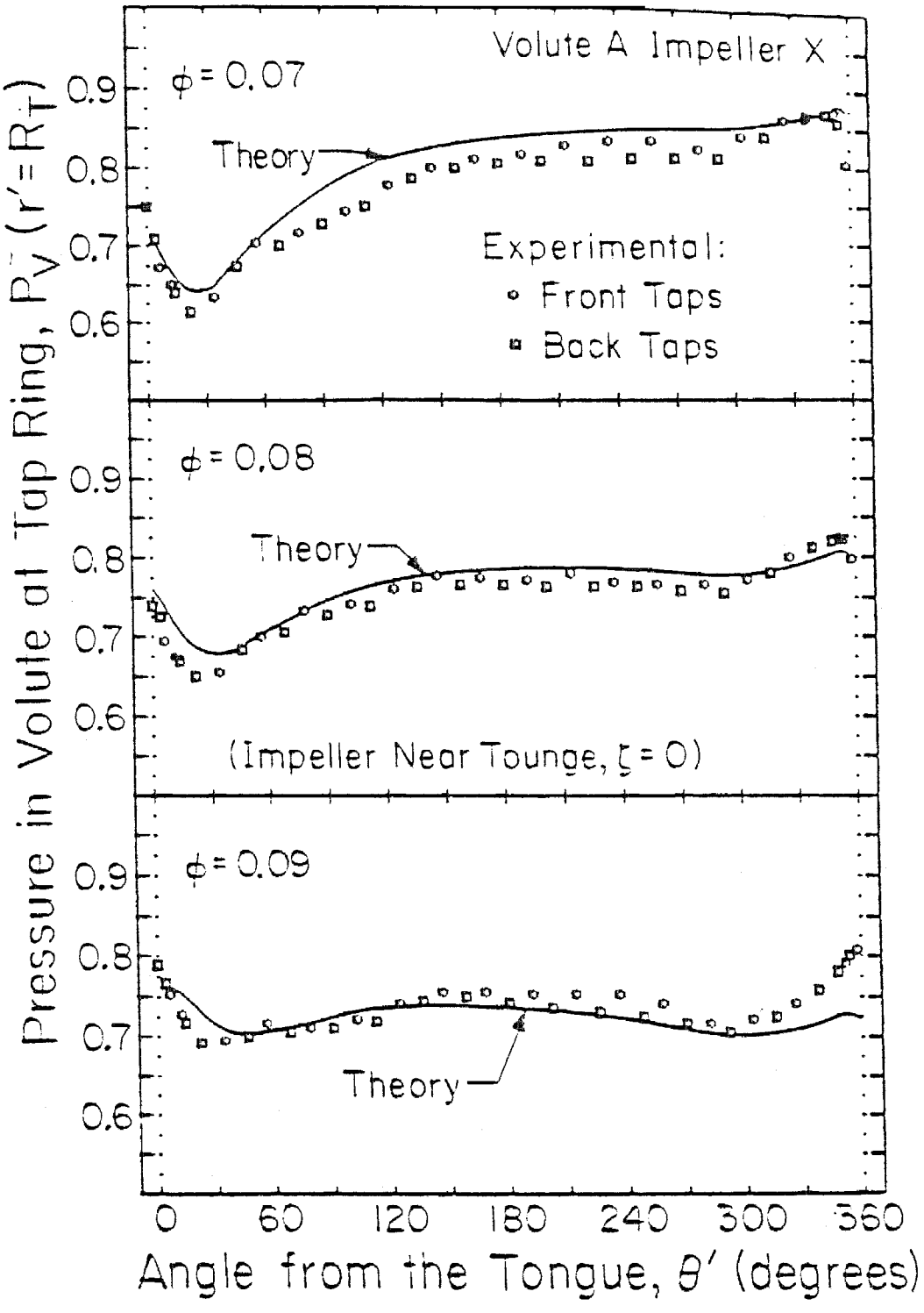

Figure 5 Comparison of experimental and theoretical discharge pressure distributions for Impeller X/Volute A (with volute rings installed) and three different flow coefficients. Pressure taps are alternately placed on front and back surfaces of volute entrance. Pressures are non-dimensionalized using $\frac{1}{2}\rho u^2 r_2^2$.

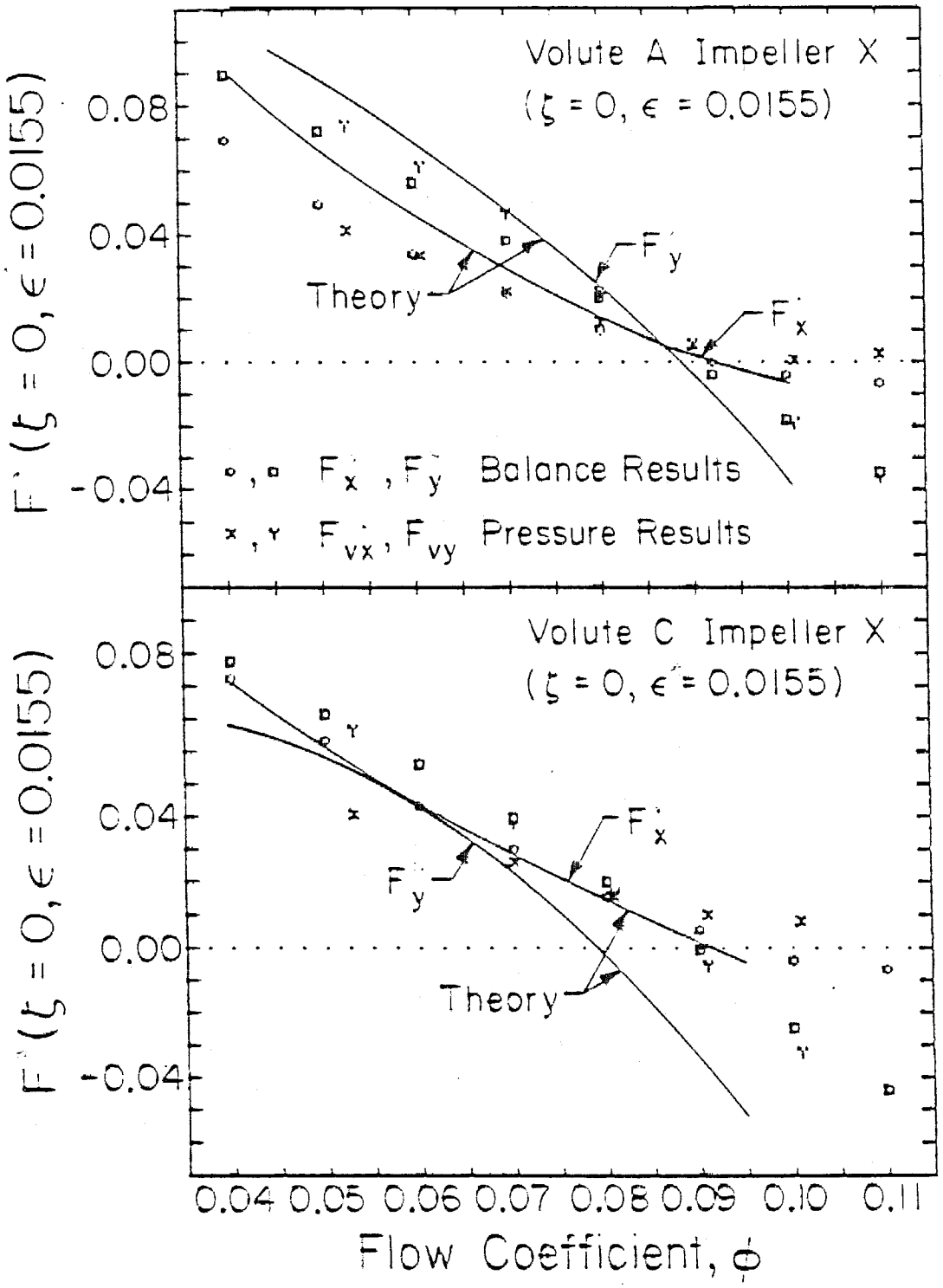

Figure 6 Radial forces for Impeller X/Volute A and for Impeller X/Volute C (both with volute rings installed) as a function of flow coefficient. Direct measurement with balance are compared with integrated pressure results and theoretical calculations.

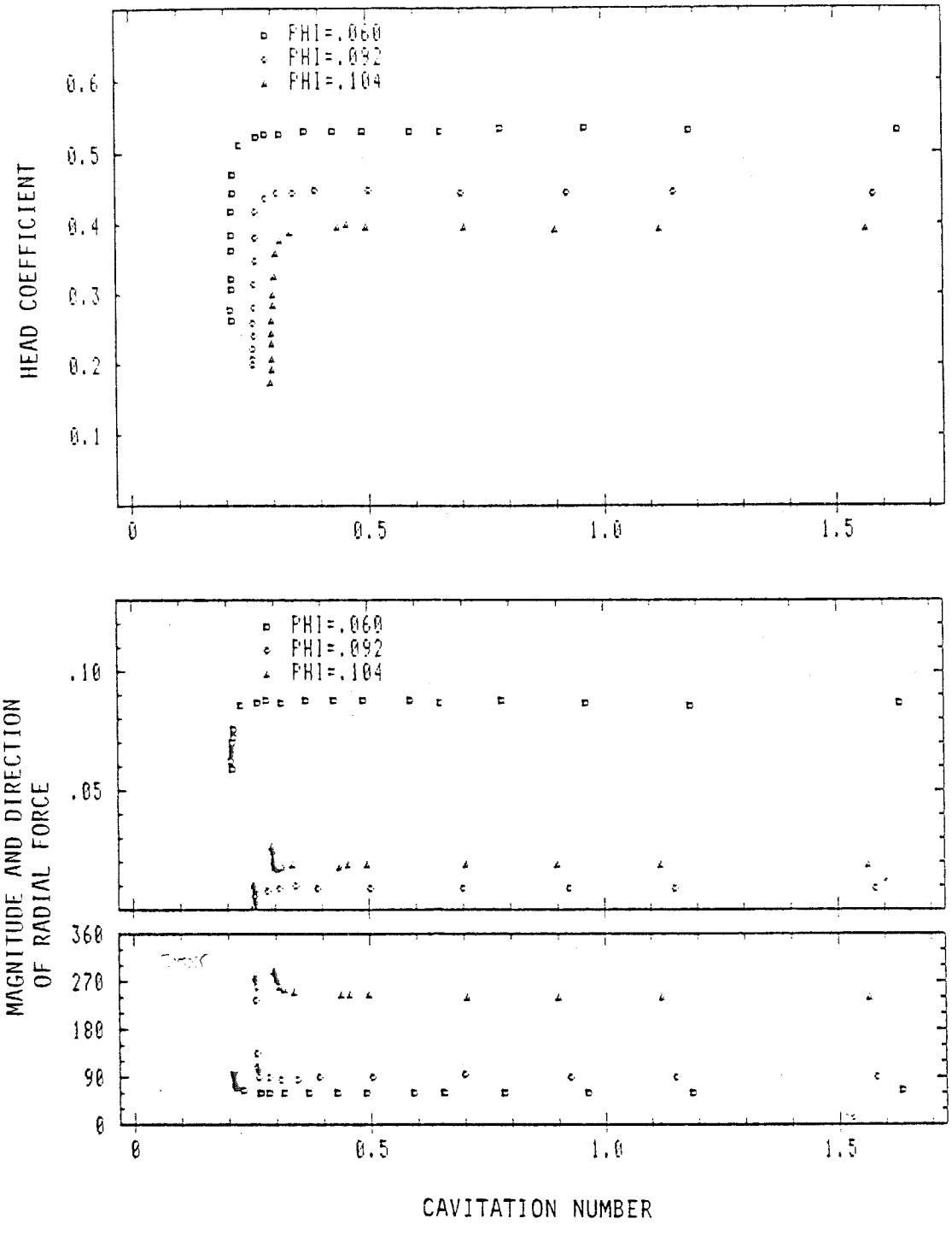

Figure 7 Upper graph: Impeller X/Volute A head coefficient plotted versus cavitation number for three different flow coefficients (□ : Φ = 0.060, ○ : Φ = 0.092, Δ = 0.104). Lower graph: corresponding data on the magnitude and direction of the radial forces as a function of cavitation number.

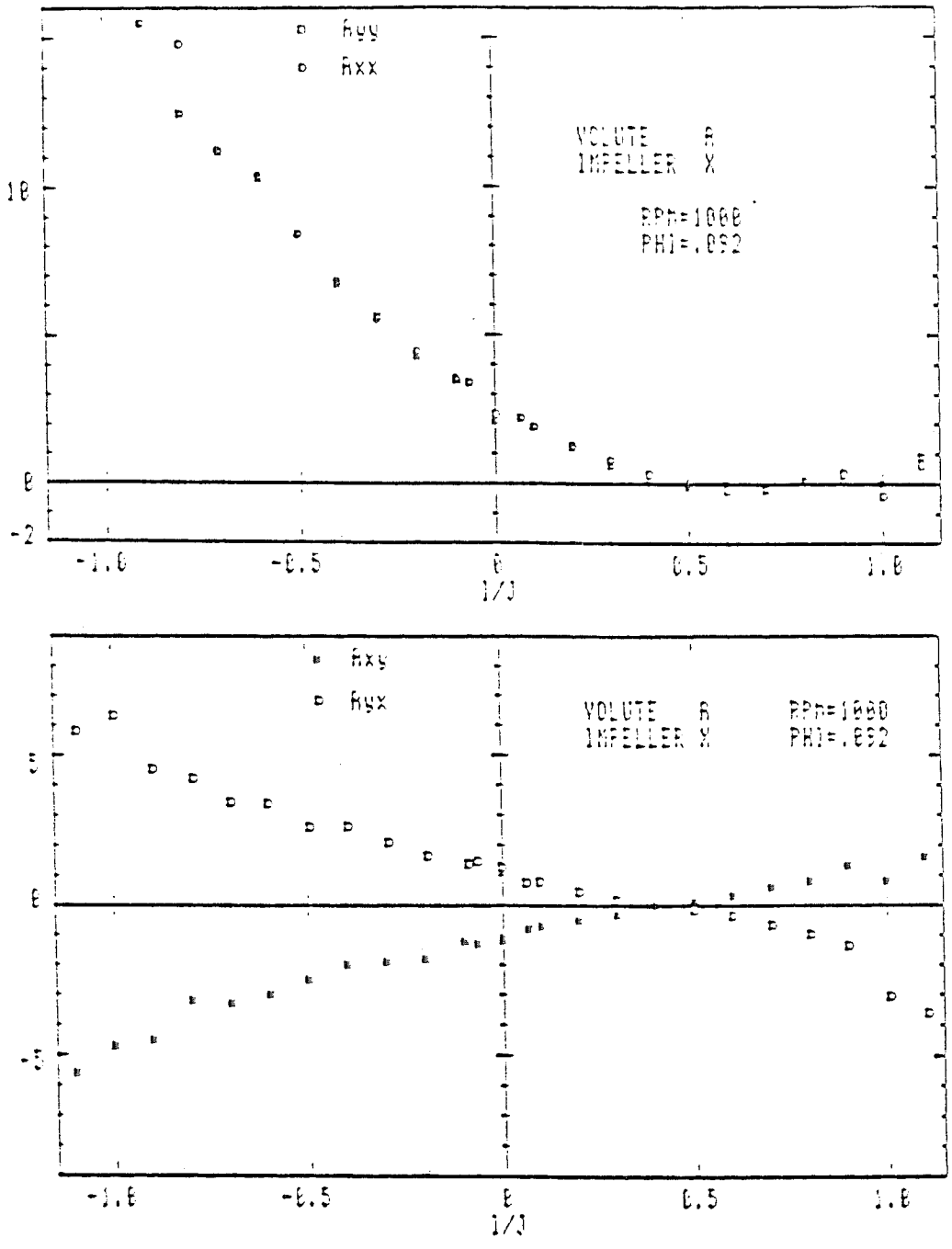

Figure 8 Hydrodynamically-induced rotordynamic matrices, [A], for Impeller X/Volute A at 1000 rpm and a flow coefficient, $\Phi = 0.092$. Plotted as function of frequency ratio, Ω/ω (or I/J).

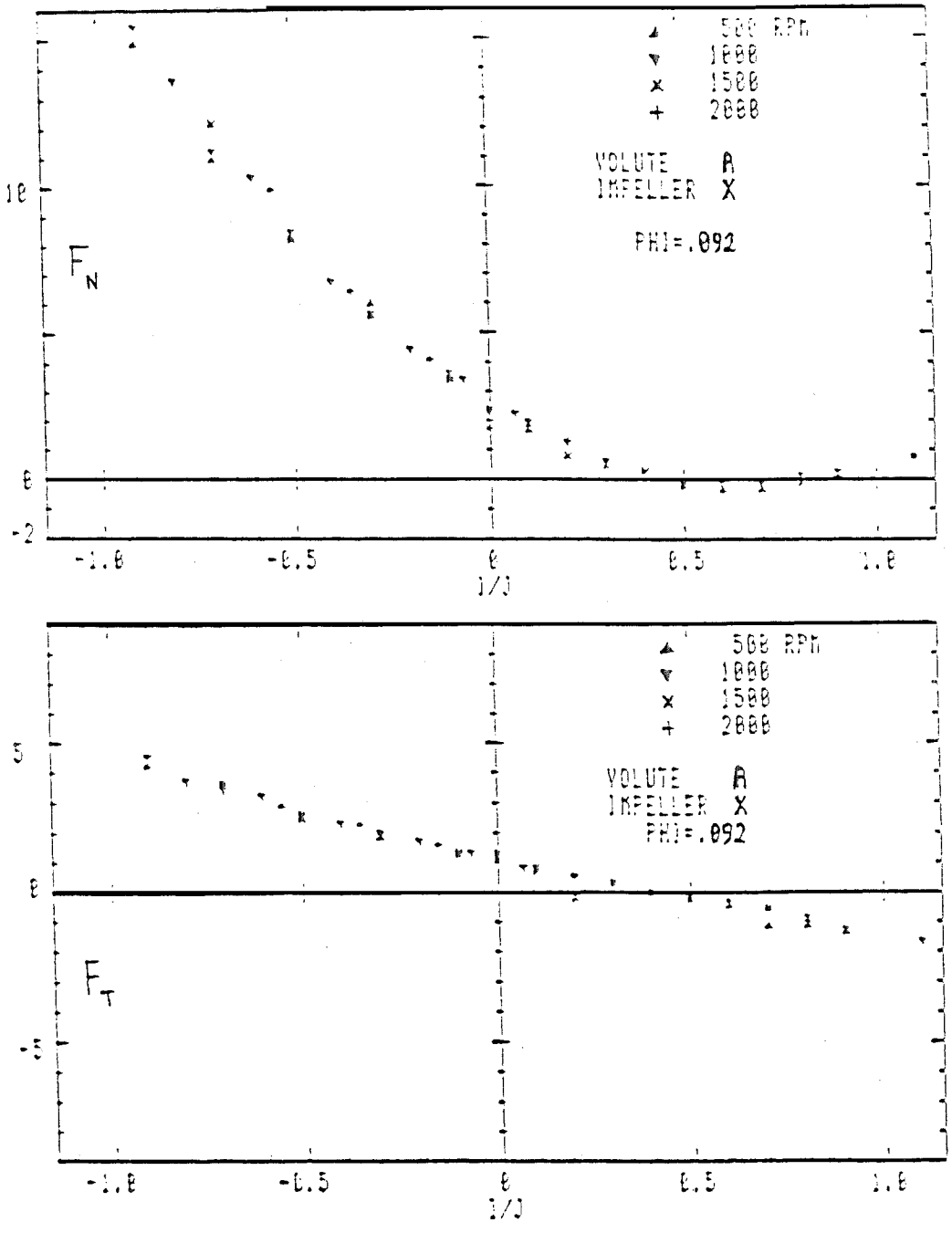

Figure 9 Normal and tangential forces, F_N and F_T, for Impeller X/ Volute A at $\Phi = 0.092$ and various shaft speeds (RPM) plotted against frequency ratio.

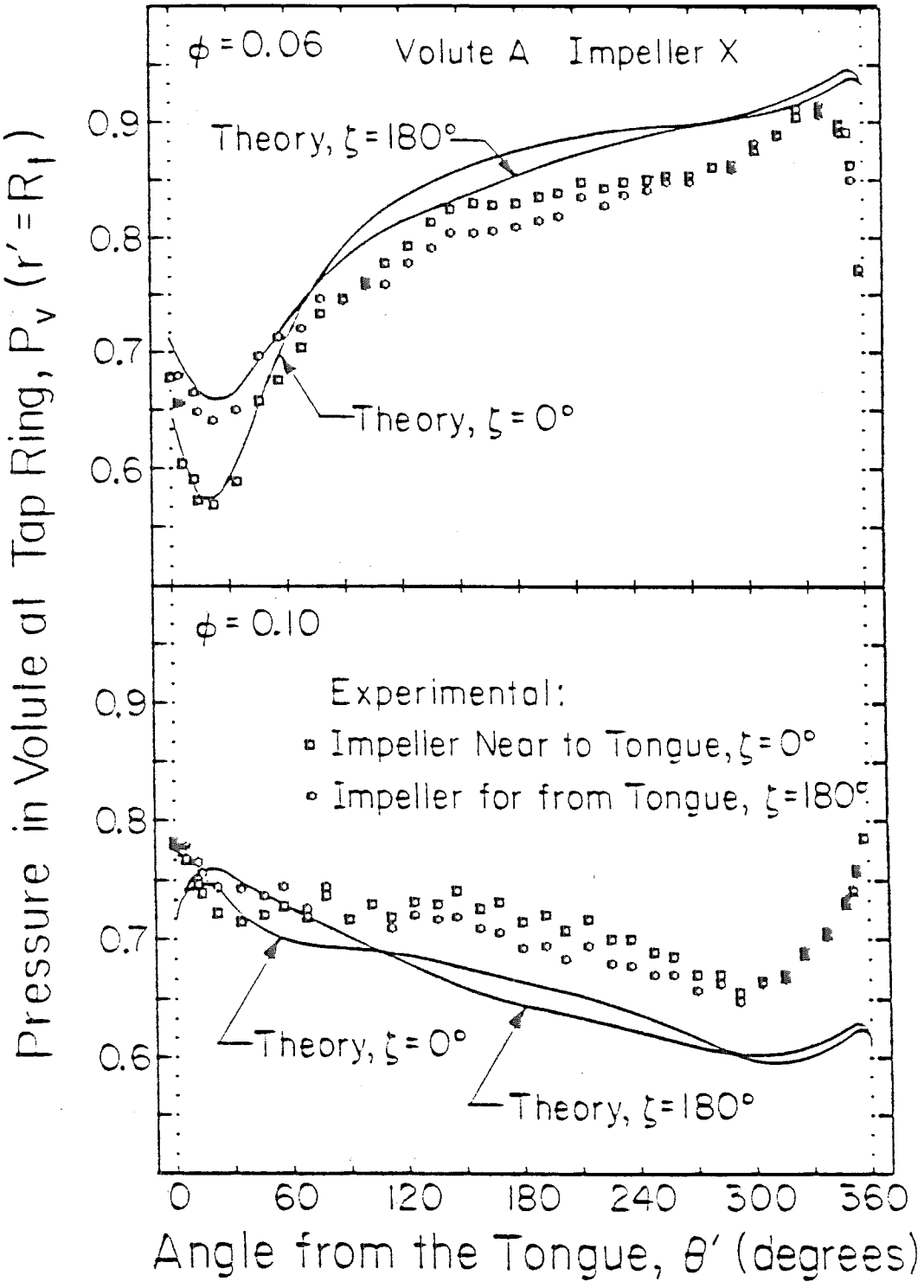

Figure 10 Typical shifts in discharge pressure distributions due to change in the position of the impeller; $\delta = 0$ corresponds to a position on current whirl orbit closest to volute tongue; $\delta = 180°$, the position furthest away. Pressures as in figure 5.

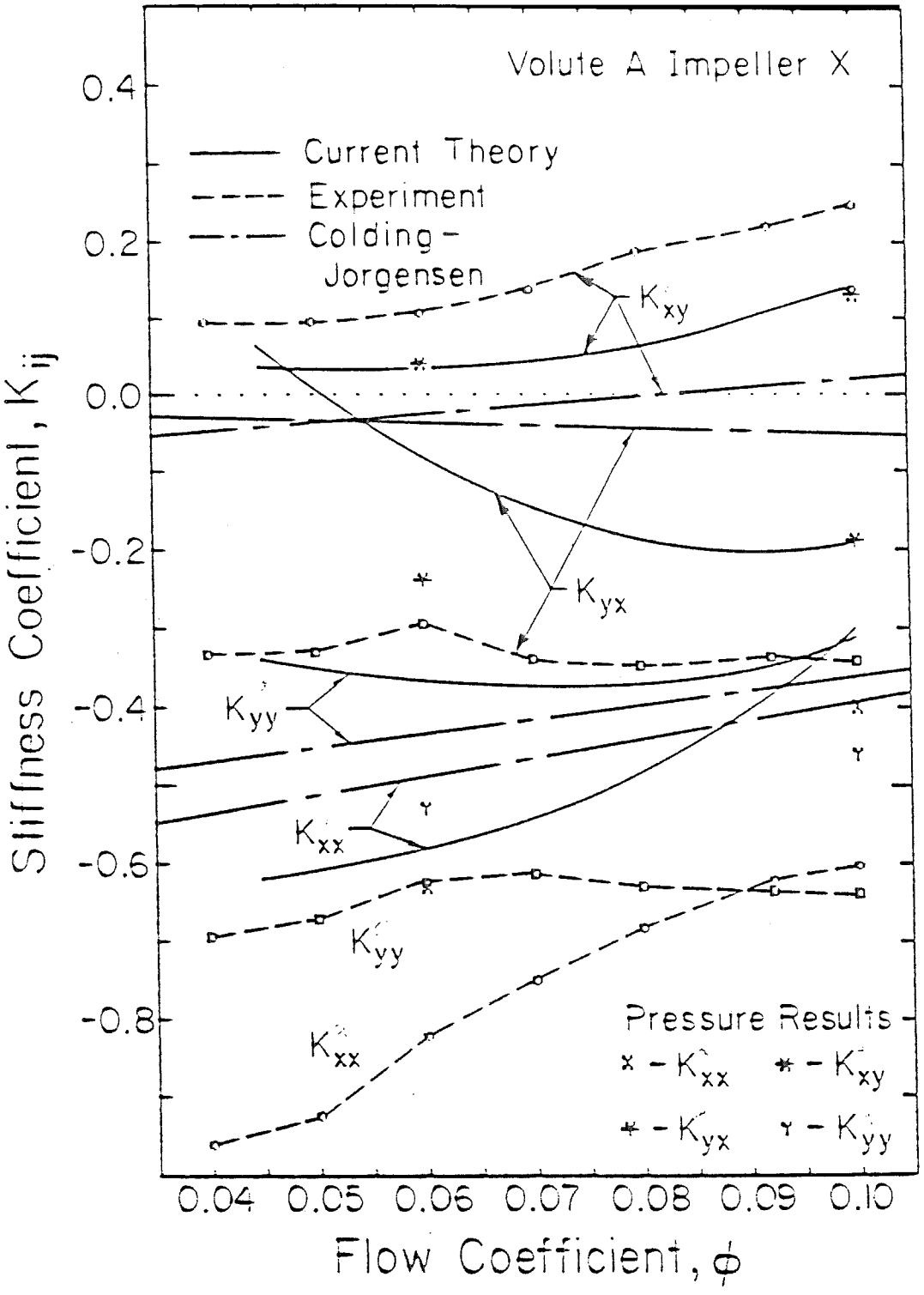

Figure 11 Stiffness matrices for Impeller X/Volute A (with volute rings installed) as a function of flow coefficient. Internal balance measurements (experiment) and integrated discharge pressure measurements are compared with results from Adkins and Brennen (current theory) and Colding-Jorgensen theories.

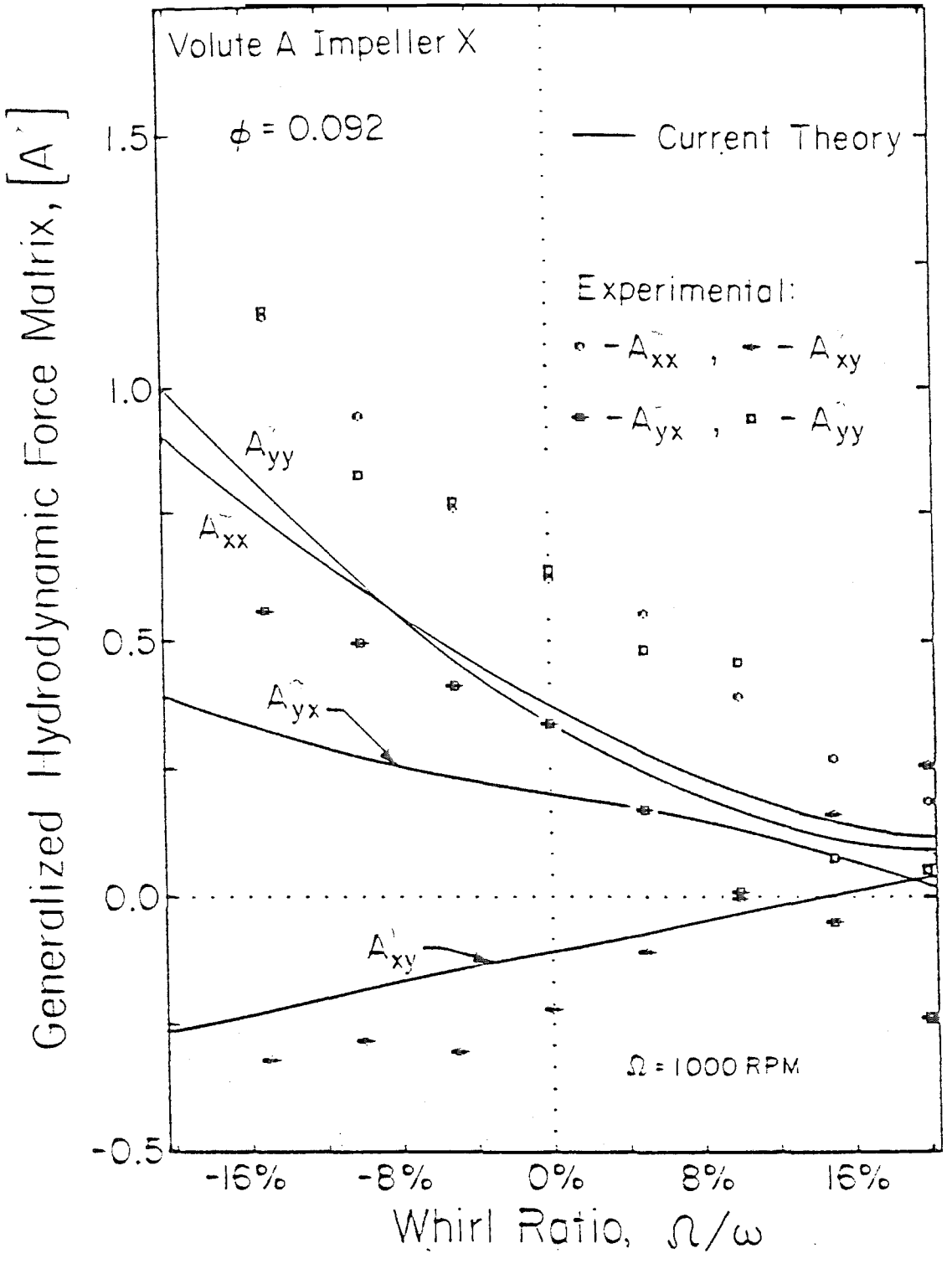

Figure 12 Rotordynamic matrices for Impeller X/Volute A (with volute rings installed) at a flow coefficient of 0.092 as a function of whirl ratio, Ω/ω. Adkins and Brennen theory compared with direct balance measurements.

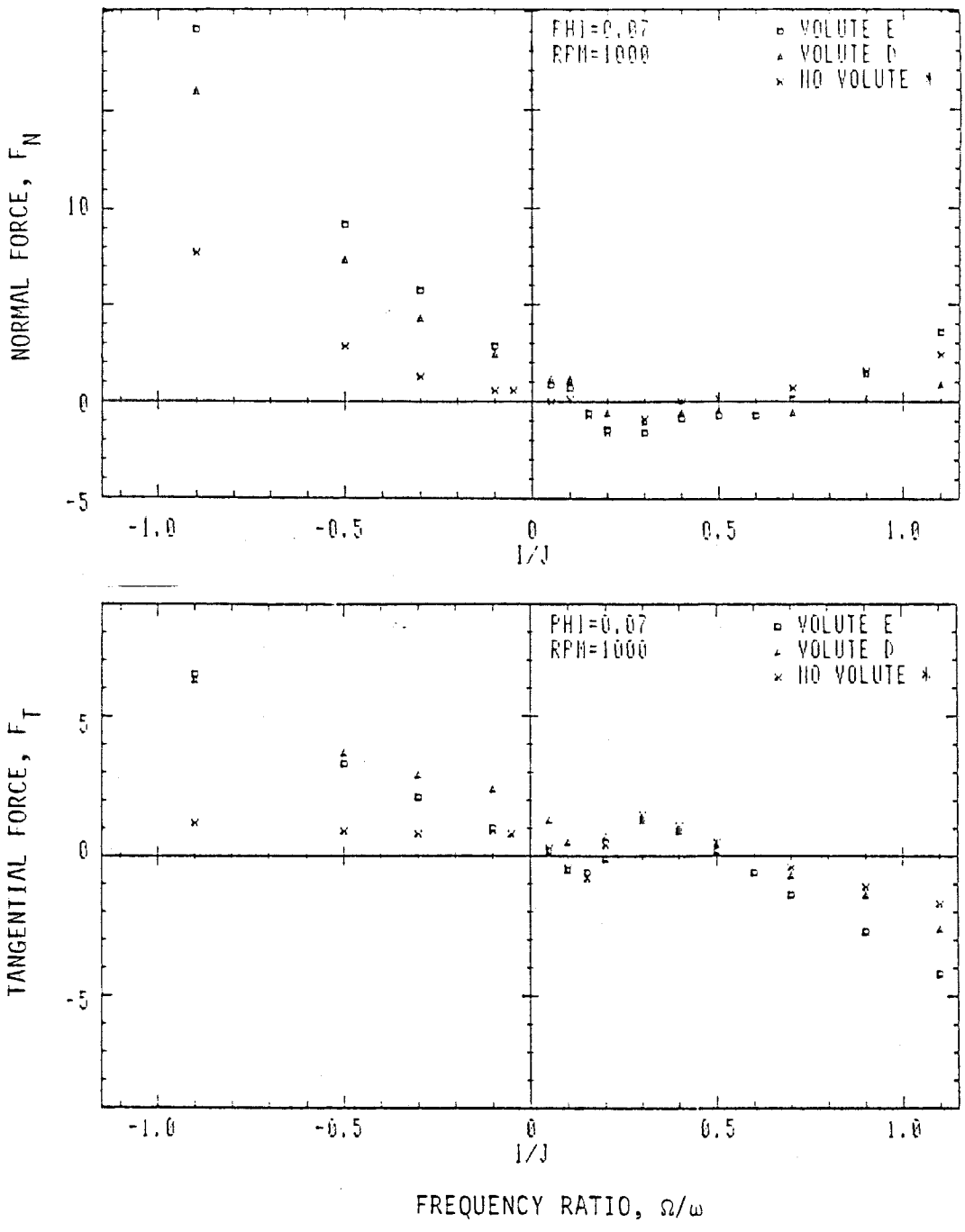

Figure 13 Normal and tangential forces for SSME Impeller R with various volutes at a flow coefficient of 0.07; plotted against frequency ratio, Ω/ω or I/J.